Absence of SPARC results in increased cardiac rupture and dysfunction after acute myocardial infarction

Mark W.M. Schellings,[1] Davy Vanhoutte,[4,6] Melissa Swinnen,[1] Jack P. Cleutjens,[2] Jacques Debets,[3] Rick E.W. van Leeuwen,[1] Jan d'Hooge,[5] Frans Van de Werf,[6] Peter Carmeliet,[4,7] Yigal M. Pinto,[1] E. Helene Sage,[8] and Stephane Heymans[1]

[1]Center for Heart Failure Research, [2]Department of Pathology, and [3]Department of Pharmacology, Cardiovascular Research Institute Maastricht (CARIM), University Hospital Maastricht, 6229 HX Maastricht, Netherlands
[4]Vesalius Research Center (VRC) and [5]Department of Cardiovascular Diseases, K.U. Leuven, 3000 Leuven, Belgium
[6]Department of Cardiology, University Hospital of Leuven, B-3000 Leuven, Belgium
[7]Vesalius Research Center (VRC), VIB, 3000 Leuven, Belgium
[8]Hope Heart Program, Benaroya Research Institute at Virginia Mason, Seattle, WA 98101

The matricellular protein SPARC (secreted protein, acidic and rich in cysteine, also known as osteonectin) mediates cell–matrix interactions during wound healing and regulates the production and/or assembly of the extracellular matrix (ECM). This study investigated whether SPARC functions in infarct healing and ECM maturation after myocardial infarction (MI). In comparison with wild-type (WT) mice, animals with a targeted inactivation of *SPARC* exhibited a fourfold increase in mortality that resulted from an increased incidence of cardiac rupture and failure after MI. *SPARC*-null infarcts had a disorganized granulation tissue and immature collagenous ECM. In contrast, adenoviral overexpression of *SPARC* in WT mice improved the collagen maturation and prevented cardiac dilatation and dysfunction after MI. In cardiac fibroblasts in vitro, reduction of SPARC by short hairpin RNA attenuated transforming growth factor β (TGF)–mediated increase of Smad2 phosphorylation, whereas addition of recombinant SPARC increased Smad2 phosphorylation concordant with increased Smad2 phosphorylation in *SPARC*-treated mice. Importantly, infusion of TGF-β rescued cardiac rupture in *SPARC*-null mice but did not significantly alter infarct healing in WT mice. These findings indicate that local production of SPARC is essential for maintenance of the integrity of cardiac ECM after MI. The protective effects of SPARC emphasize the potential therapeutic applications of this protein to prevent cardiac dilatation and dysfunction after MI.

CORRESPONDENCE
Stephane Heymans:
s.heymans@cardio.unimaas.nl

Abbreviations used: ECM, extracellular matrix; LV, left ventricle; MI, myocardial infarction; mRNA, messenger RNA; shRNA, short hairpin RNA; SMC, smooth muscle cell.

SPARC (secreted protein, acidic and rich in cysteine, also called osteonectin and BM-40) belongs to the group of matricellular proteins, which are nonstructural proteins present in the extracellular matrix (ECM). Although they do not contribute directly to tissue integrity, they are potent modulators of cellular function. SPARC is involved in tumor progression and wound healing via its regulation of cell–ECM interactions and ECM production (1, 2). Expression of SPARC is increased after myocardial infarction (MI) and is spatially and temporally related to the formation of a fibrous scar (3, 4). Although previous studies indicate a role for SPARC in cutaneous wound healing (5, 6), evidence for a specific role for SPARC in granulation and ECM formation in an infarcted heart is lacking.

Healing after MI requires a tightly regulated process of wound healing and scar formation that consists of three overlapping phases. The initial inflammatory phase for removal of dead tissue is followed rapidly by the formation of granulation tissue, which is rich in leukocytes,

M.W.M. Schellings and D. Vanhoutte contributed equally to this paper.

The Rockefeller University Press $30.00
J. Exp. Med. Vol. 206 No. 1 113-123
www.jem.org/cgi/doi/10.1084/jem.20081244

new vessels, and proliferating fibroblasts. The final, maturation phase is characterized by a regression of granulation tissue and a progressive maturation of the collagenous ECM. Alterations in this well orchestrated response to myocardial necrosis leads to adverse infarct healing, cardiac rupture, and cardiac dysfunction (7). SPARC modulates ECM turnover in part through its effect on collagen synthesis, extracellular proteases, and growth factors (1). In addition, SPARC binds to TGF-β receptor type II in the presence of TGF-β and thereby affects its downstream signaling in mesangial cells (8).

Because SPARC is increased after MI and can affect ECM organization, we hypothesized that SPARC regulates infarct healing and ECM maturation after MI and might thereby protect against cardiac rupture and dysfunction. Our data reveal that loss of *SPARC* results in the formation of a disorganized scar and immature collagen matrix after MI. Adverse infarct healing in *SPARC*-null hearts evolves into increased cardiac rupture and dysfunction, whereas adenoviral overexpression of *SPARC* protects against cardiac dilatation and failure after MI. SPARC is therefore a promising target to obtain proper infarct healing and collagen maturation and prevent cardiac rupture, dilatation, and dysfunction after MI.

RESULTS

SPARC expression is induced after MI

To assess the expression of SPARC in the cardiac healing process, we examined SPARC protein expression in myocardial tissue of WT mice after MI. Immunoblotting of SPARC in noninfarcted remote left ventricle (LV) only revealed a moderate increase of SPARC protein expression at 3 d after MI (Fig. 1 A). In contrast, and concordant with previous findings (3, 4), SPARC protein levels were strongly increased in the infarcted LV at 7 and 14 d after MI (Fig. 1 A). Immunohistochemistry confirmed that SPARC was low to absent in sham-operated (Fig. 1 B) and in noninfarcted remote LV (Fig. 1 C) but abundantly present in the infarcted LV (Fig. 1, C and D). Double immunohistochemistry revealed that SPARC mainly colocalized with α–smooth muscle actin–positive cells (infiltrating myofibroblast; Fig. 1, E–G) and CD45-immunoreactive leukocytes (Fig. 1, H–J). Thus, SPARC protein showed a localized deposition contemporaneous with the formation of granulation tissue and progressive maturation of the infarct scar.

Increased SPARC after MI protects against cardiac rupture and dysfunction

To evaluate the function of SPARC in ECM maturation, we used a model of permanent coronary occlusion. The absence of *SPARC* was associated with a significantly increased incidence of cardiac rupture after MI: 41% (13/32) of *SPARC*-null mice (males, 8/12; females, 5/20) compared with 9% (3/34) of WT mice (males, 2/14; females, 1/20) died as a result of cardiac rupture (Fig. 2, A–C). Increased lung weight/body weight ratios at 3 d after MI in *SPARC*-null compared with WT mice pointed toward cardiac dysfunction in *SPARC*-null mice (Table I). Four male SPARC-null mice that did not die from cardiac rupture displayed severe shortness of breath within 7 d. Two of them died prematurely (6 d after MI), whereas the other two were killed after echocardiography at 7 d after MI. The fractional shortening of these two mice pointed toward severe systolic dysfunction (7.1 ± 3.9%), which was associated with significantly increased lung weight/body weight ratios in the four male *SPARC*-null mice surviving

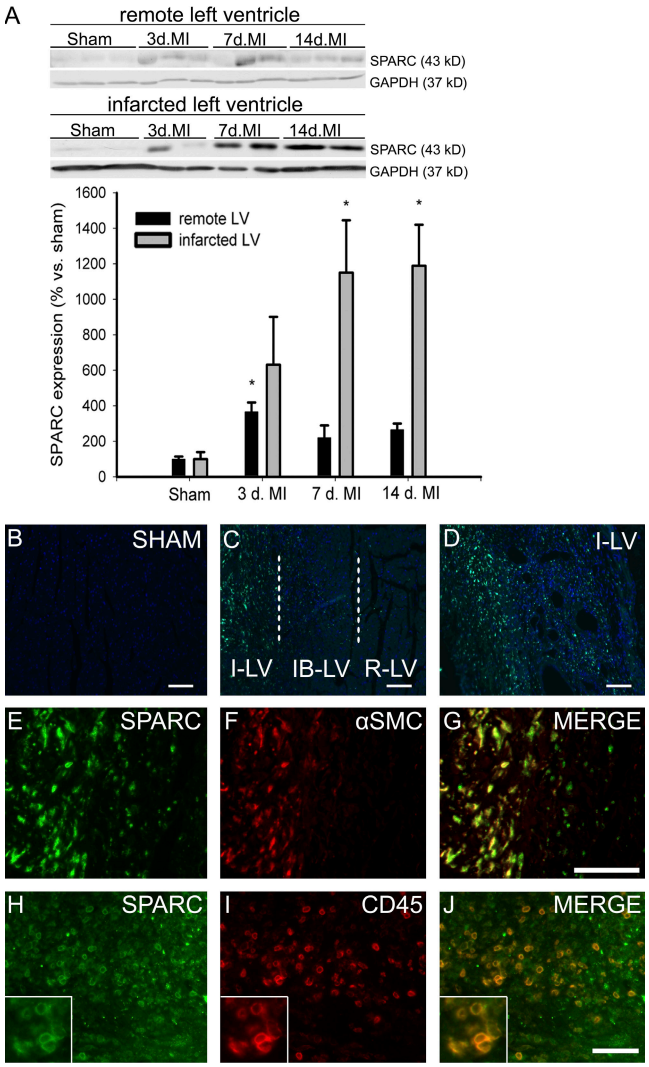

Figure 1. SPARC expression is induced after MI. (A) SPARC protein is increased after MI in mice. Representative Western blots of SPARC in remote and infarcted LV from WT mice at 3, 7, and 14 d after MI (n = 4 per time point; *, $P < 0.05$). (B–D) SPARC immunofluorescent staining (green) is absent in sham-operated hearts (B) and remote LV (R-LV), gradually increases in the infarct border LV (IB-LV; C), and is strongly up-regulated in the infarcted LV (I-LV) 7 d after MI (C and D). (E–J) SPARC expression (E and H) colocalizes with α–smooth muscle cell (SMC) actin–positive myofibroblasts (F and G) and CD45 immunoreactive leukocytes (I and J) in the infarcted LV of WT infarcted hearts 7 d after MI. The insets in H–J show detailed SPARC and CD45 immunoreactive leukocytes. Error bars represent the mean ± SEM. Bars: (B–D, H, and J) 100 µm; (E–G) 50 µm.

cardiac rupture (14.1 ± 0.7 vs. 9.7 ± 1.3 in WT mice; $P < 0.05$).

Left ventricular pressure and heart rate were similar in sham-operated and infarcted WT and *SPARC*-null mice at baseline. Systolic function, as measured by echocardiography, was reduced in infarcted compared with sham-operated mice at 3, 7, and 14 d after MI but to a similar extent in both genotypes (Table I). Baseline dP/dt_{max} and dP/dt_{min} did not differ between infarcted female *SPARC*-null and WT mice at 14 d after MI (Fig. 2, D and E). However, hemodynamic stress induced by dobutamine increased contractility and relaxation in infarcted female WT mice but to a lesser extent in female *SPARC*-null mice (Fig. 2, D and E). Systolic blood pressure and heart rate did not differ significantly after dobutamine infusion between infarcted female WT and *SPARC*-null mice (Fig. 2, F and G). Although *SPARC* deficiency does

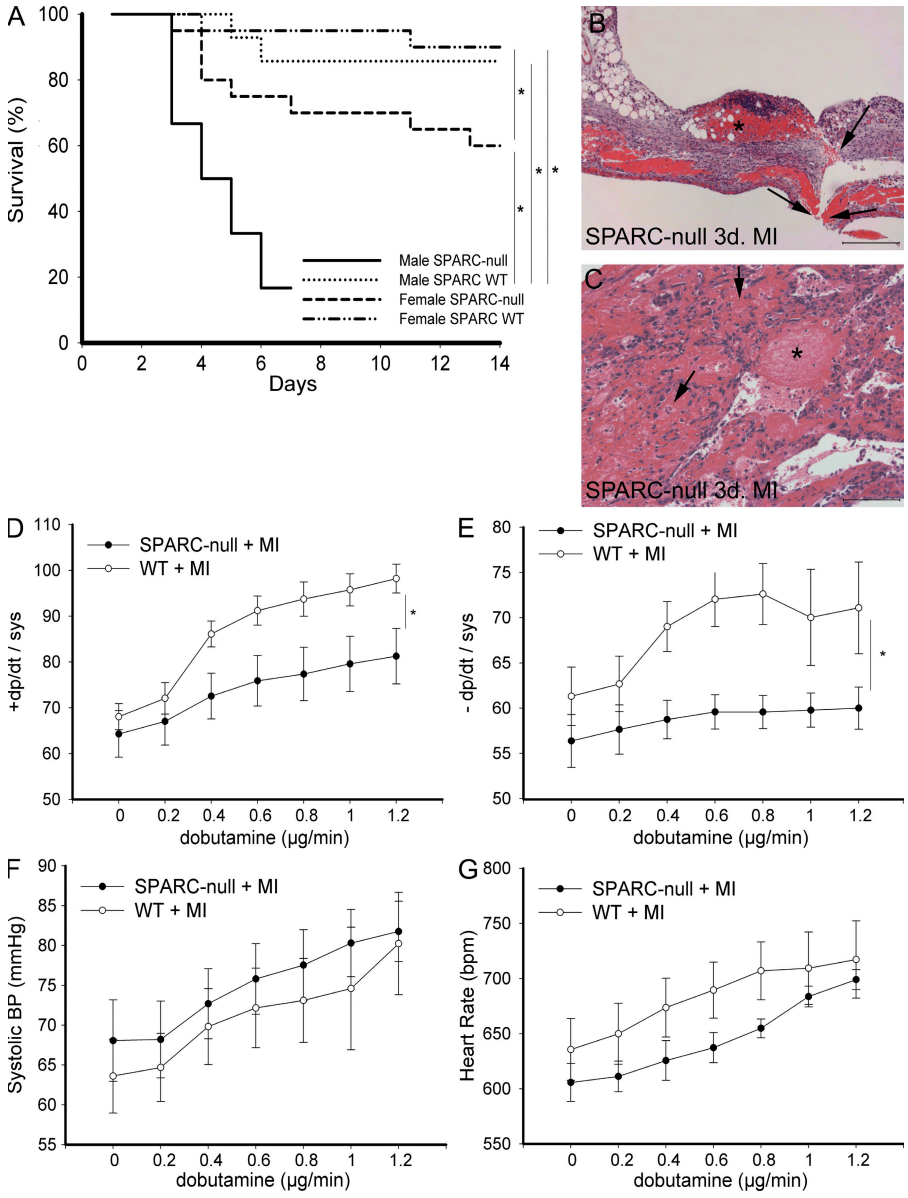

Figure 2. Absence of *SPARC* results in cardiac rupture and dysfunction. (A) Kaplan-Meier curve showing that targeted deletion of *SPARC* resulted in decreased survival of *SPARC*-null (mainly male) compared with WT mice after MI (*, $P < 0.05$). Decreased survival was mainly caused by cardiac rupture. Two male SPARC-null mice had to be killed at 7 d after MI because of severe shortness of breath and, therefore, were not included in the survival curve. (B and C) Histological analysis of ruptured LV of male *SPARC*-null infarcted hearts (hematoxylin and eosin stained) revealing rupture site (B, arrows), intramural hemorrhages of the infarcted ventricular wall (C, arrows), and massive infiltration of erythrocytes and inflammatory cells (C) and thrombi (B and C, asterisks) at 3 d after MI. (D–G) Decreased survival is associated with depressed cardiac contractility (D) and relaxation (E) during infusion of dobutamine in *SPARC*-null female ($n = 7$) in comparison with female WT ($n = 9$) mice 14 d after MI, whereas systolic blood pressure (BP; F) and heart rate (G) did not differ significantly (*, $P < 0.05$). bpm, beats per minute. Error bars represent the mean ± SEM. Bars: (B) 200 µm; (C) 100 µm.

Table I. Functional analysis of WT and *SPARC*-null mice after MI

	Sham		MI, 3 d		MI, 7 d		MI, 14 d	
	WT, *n* = 12 (M/F: 6/6)	null, *n* = 13 (M/F: 4/9)	WT, *n* = 10 (M/F: 5/5)	null, *n* = 11 (M/F: 5/6)	WT, *n* = 7 (M/F: 3/4)	null, *n* = 7 (F: 7)	WT, *n* = 9 (F: 9)	null, *n* = 9 (F: 9)
FS (%)	26 ± 1.3	30 ± 2.2	14 ± 3.1[b]	16 ± 2.6[b]	18 ± 3.1[b]	15 ± 7[b]	12 ± 1.4[b]	12 ± 1.2[b]
LVIDd (mm)	3.7 ± 0.1	3.6 ± 0.1	4.2 ± 0.2[b]	4.1 ± 0.2[b]	4.7 ± 0.2[b]	4.9 ± 0.5[b]	5.0 ± 0.3[b]	5.3 ± 0.2[b]
LVIDs (mm)	2.8 ± 0.1	2.5 ± 0.1	3.6 ± 0.2[b]	3.5 ± 0.2[b]	3.9 ± 0.3[b]	4.3 ± 0.6[b]	4.4 ± 0.3[b]	4.7 ± 0.3[b]
PWd (mm)	1.0 ± 0.1	0.9 ± 0.1	0.7 ± 0.1[b]	0.8 ± 0.1[b]	0.8 ± 0.1	0.9 ± 0.1	1.0 ± 0.1	1.0 ± 0.1
IVSd (mm)	0.9 ± 0.1	1.0 ± 0.1	0.7 ± 0.1[b]	0.9 ± 0.1[a]	1.0 ± 0.2	0.9 ± 0.1	0.8 ± 0.1	0.8 ± 0.1
HW/BW	5.2 ± 0.2	5.2 ± 0.2	5.6 ± 0.2	5.8 ± 0.3	7.0 ± 0.3[b]	7.9 ± 0.8[b]	6.4 ± 0.1[b]	7.2 ± 0.3[ab]
LW/BW	6.4 ± 0.4	5.9 ± 0.2	6.4 ± 0.2	7.4 ± 0.3[ab]	9.7 ± 1.3[b]	10 ± 1.2[b]	10 ± 1.3[b]	9.8 ± 1.2[b]

M, male; F, female; FS, fractional shortening; LVIDd, left ventricular internal diameter diastole; PWd, posterior wall diastole; IVSd, intraventricular septum diastole; HW, heart weight; BW, body weight; and LW, lung weight.
[a]$P < 0.05$ in SPARC-null versus WT infarcts.
[b]$P < 0.05$ in infarcted versus sham.

not affect cardiac structure or performance of the heart under physiological conditions, increased levels of SPARC appear to play a pivotal role in the healing process by maintenance of the structural integrity of the heart after MI.

To investigate whether the absence of *SPARC* or gender differences resulted in compensatory changes in expression of SPARC-related factors before the onset of cardiac rupture, we determined transcript levels in male and female sham and 3-d-old infarcted hearts of *SPARC*-null and WT mice. SMOC1, SMOC2, and Hevin were selected because previous studies described their expression in the heart (9–11), but little is known about the biological function of these proteins in the heart. Interestingly, transcript levels of *SMOC2* were significantly increased in WT and *SPARC*-null female sham mice in comparison with male sham mice, whereas its expression decreased significantly after MI with no significant differences between the genders (Table II). In contrast, *SMOC1* expression significantly increased 3 d after MI but did not significantly differ between the genders or genotypes. Transcript levels of *Hevin* slightly decreased after MI, reaching significance in the infarcted female WT mice in comparison with the respective sham. Finally, *SPARC* transcript levels significantly increased at 3 d after MI in WT mice but did not significantly differ between the genders (Table II).

SPARC-null infarcts exhibit disorganized granulation tissue and deficient scar maturation

Infarct size did not significantly differ between WT and *SPARC*-null mice (Table III). Histopathological analysis of infarcts revealed a disorganized scar tissue with diffuse RBC infiltration in *SPARC*-null infarcts (Fig. 3, A–D). Adverse infarct healing in *SPARC*-null mice was not related to significant differences in inflammation or vascular density, except for the area of myofibroblasts, which was significantly increased in *SPARC*-null infarcts (Table III).

Sirius red polarization microscopy of collagen fibers revealed a predominance of loosely assembled (yellow-green) collagen fibers in *SPARC*-null infarcts at 14 d (ratio of orange-red/yellow-green birefringent collagen), which was in contrast to the well aligned and thick tightly packed (orange-red) fibers in WT infarcts (Fig. 3, E–H; Table III). Ultrastructural analysis confirmed a disorganized and immature collagen matrix in *SPARC*-null infarcts, as indicated by the decreased diameter of collagen fibrils, which was in contrast to the well structured collagen matrix in WT infarcts (Fig. 3, I–K). Ultrastructural and histological analysis of the cardiac matrix in *SPARC*-null and WT sham mice did not reveal significant differences.

The absence of *SPARC* did not affect collagen synthesis, as is shown by the lack of significant differences in the fraction

Table II. Transcript levels of SPARC-related factor messenger RNAs (mRNAs)

	Sham				3-d MI			
	WT M (*n* = 7)	WT F (*n* = 7)	KO M (*n* = 7)	KO F (*n* = 7)	WT M (*n* = 6)	WT F (*n* = 8)	KO M (*n* = 5)	KO F (*n* = 10)
SMOC1	11 ± 1.1	12 ± 1.5	13 ± 4.3	11 ± 1.4	35 ± 6.8[a]	34 ± 5.3[a]	26 ± 6.4[a]	27 ± 5.4[a]
SMOC2	5.0 ± 0.9	10 ± 0.5[b]	7.3 ± 0.6	9.3 ± 0.3[b]	3.4 ± 0.5	3.0 ± 0.5[a]	4.2 ± 0.7[a]	4.8 ± 0.6[ac]
Hevin	1.0 ± 0.1	1.2 ± 0.1	1.0 ± 0.1	0.8 ± 0.1[c]	0.8 ± 0.1	0.7 ± 0.1[a]	0.6 ± 0.1	0.7 ± 0.1
SPARC	3.4 ± 1.5	1.8 ± 0.1	ND	ND	14 ± 1.6[a]	16 ± 1.8[a]	ND	ND

M, male; F, female; ND, not detectable. Numbers are in arbitrary units.
[a]$P < 0.05$ in MI group versus respective sham.
[b]$P < 0.05$ between males and females of the same genotype.
[c]$P < 0.05$ between WT and SPARC-null mice of the same gender.

Table III. Histological analysis of the infarcted area

	WT 7d (n = 8)	*SPARC*-null, 7d (n = 7)	WT + TGF-β, 7d (n = 6)	*SPARC*-null + TGF-β, 7d (n = 6)	WT, 14 d (n = 10)	*SPARC*-null, 14 d (n = 11)
Infarct size (%)	43 ± 3.6	46 ± 4.1	38 ± 3	36 ± 4	42 ± 2.6	43 ± 2.7
Residual necrotic area (%)	9.6 ± 1.8	9.6 ± 2.2	14.3 ± 6.9	3.9 ± 1.7	2.7 ± 0.7	1.0 ± 0.3[a]
Infarct thickness (μm)	380 ± 61	290 ± 22	430 ± 40	560 ± 72[b]	390 ± 27	380 ± 27
Leukocyte infiltration (cells/mm^2)	870 ± 180	820 ± 140	720 ± 180	870 ± 80	660 ± 130	270 ± 68[a]
Coronary growth (vessels/mm^2)	42 ± 4	45 ± 5	59 ± 5[b]	59 ± 3[b]	54 ± 10	43 ± 5
Capillary growth (vessels/mm^2)	89 ± 14	119 ± 18	135 ± 31	143 ± 23	87 ± 16	116 ± 13
Myofibroblast (% area)	2.1 ± 0.4	3.8 ± 0.8[a]	1.7 ± 0.1	1.1 ± 0.2[b]	0.8 ± 0.4	1.6 ± 0.2
Collagen deposition (%)	26 ± 2.5	20 ± 3.6	28 ± 2	30 ± 2[b]	36 ± 2.4	37 ± 2.0
Ratio O-R thick/Y-G thin collagen fibers	11 ± 2.3	2.5 ± 0.5[a]	20 ± 2.9[b]	4.5 ± 1.2[b]	17 ± 1.8	8.1 ± 1.8[a]

O-R, orange-red; Y-G, yellow-green.
[a]$P < 0.05$ in SPARC-null versus WT infarcts at corresponding time after MI.
[b]$P < 0.05$ in TGF-β–treated infarcts versus untreated infarcts at the corresponding time after MI.

Sirius red–stained collagen (Fig. 3, E and G; Table III) or transcript levels of *collagen type I* and *type III* (Table S1, available at http://www.jem.org/cgi/content/full/jem.20081244/DC1) in *SPARC*-null compared with WT infarcts. Thus, increased cardiac rupture and dysfunction in *SPARC*-null mice are related, at least in part, to deficient maturation of the scar after MI.

Adenoviral overexpression of *SPARC* protects against cardiac dilatation and dysfunction after acute MI

To investigate whether overexpression of *SPARC* could prevent cardiac dysfunction after MI, we enhanced *SPARC* expression in WT mice by injection of a replication-deficient adenovirus harboring mouse *SPARC* (AdSPARC) 2 d before MI. Subsequently, there was a 2.8-fold increase in expression of SPARC in plasma and a 2.6-fold increase of SPARC expression in the infarct area at 14 d after MI in comparison to control AdR5-injected mice (Fig. 4, A and B). The increased levels of SPARC prevented cardiac dilatation and dysfunction after MI (Table IV) without alteration of infarct size (Table V). SPARC significantly increased collagen deposition and birefringence in the infarct zone (Fig. 4, C-F; Table V) but did not affect the amount of CD45-positive leukocytes, α–smooth muscle actin–positive myofibroblasts, and coronary vessels in comparison to control AdR5-treated mice (Table V). These findings were corroborated by the increased transcript levels of ECM proteins in the infarcts of mice treated with AdSPARC (Table S2, available at http://www.jem.org/cgi/content/full/jem.20081244/DC1). Thus, overexpression of *SPARC* protects against adverse collagen remodeling, which is associated with reduced ventricular dilatation and failure after MI.

SPARC modulates TGF-β signaling

We asked whether the increased collagen deposition found in the infarcts of SPARC-overexpressing mice was associated with altered signaling of TGF-β, which is a known profibrotic cytokine (12). The levels of phosphorylated and total Smad2 were significantly higher in the infarcts of AdSPARC-treated WT mice (Fig. 5 A). These results were concordant with experiments in vitro, which showed that addition of recombinant SPARC increased Smad2 phosphorylation at baseline as well as after stimulation with TGF-β1 (Fig. 5 B). Inhibition of SPARC by short hairpin RNA (shRNA) resulted in an 80% decrease in levels of SPARC protein (Fig. 5 C). Although treatment with 1 ng/ml TGF-β resulted in a significant increase in the ratio of phosphorylated Smad2 (p-Smad2) to total Smad2 protein in control fibroblasts (100 ± 4% in control compared with 272 ± 30% in TGF-β–treated fibroblasts; $n = 5$; $P < 0.05$), the decrease in SPARC significantly blunted the ratio of p-Smad2/Smad2 at baseline (66 ± 8%; $n = 6$; $P < 0.05$ compared with WT fibroblasts) and after treatment with TGF-β (234 ± 14%; $n = 5$; $P < 0.05$ compared with TGF-β–treated WT fibroblasts; Fig. 5 C). We did not find significant differences in Smad2 phosphorylation between WT and *SPARC*-null infarcts, a result which might reflect the increased presence of myofibroblasts in the *SPARC*-null infarcts. Together, these data confirm a role for SPARC in the regulation of TGF-β signaling.

Infusion of TGF-β protects against cardiac rupture in *SPARC*-null mice

TGF-β is strongly implicated in infarct healing and remodeling after MI. To investigate whether aberrant TGF-β signaling in the absence of *SPARC* is involved in the adverse infarct healing and increased cardiac rupture after MI observed in *SPARC*-null animals, *SPARC*-null and WT mice were treated with TGF-β.

Administration of TGF-β significantly improved the survival of *SPARC*-null animals by its diminution of cardiac rupture (1 out of 7 in TGF-β–treated compared with 8 out of 12 in saline-treated *SPARC*-null mice; Fig. 5 D). Histological

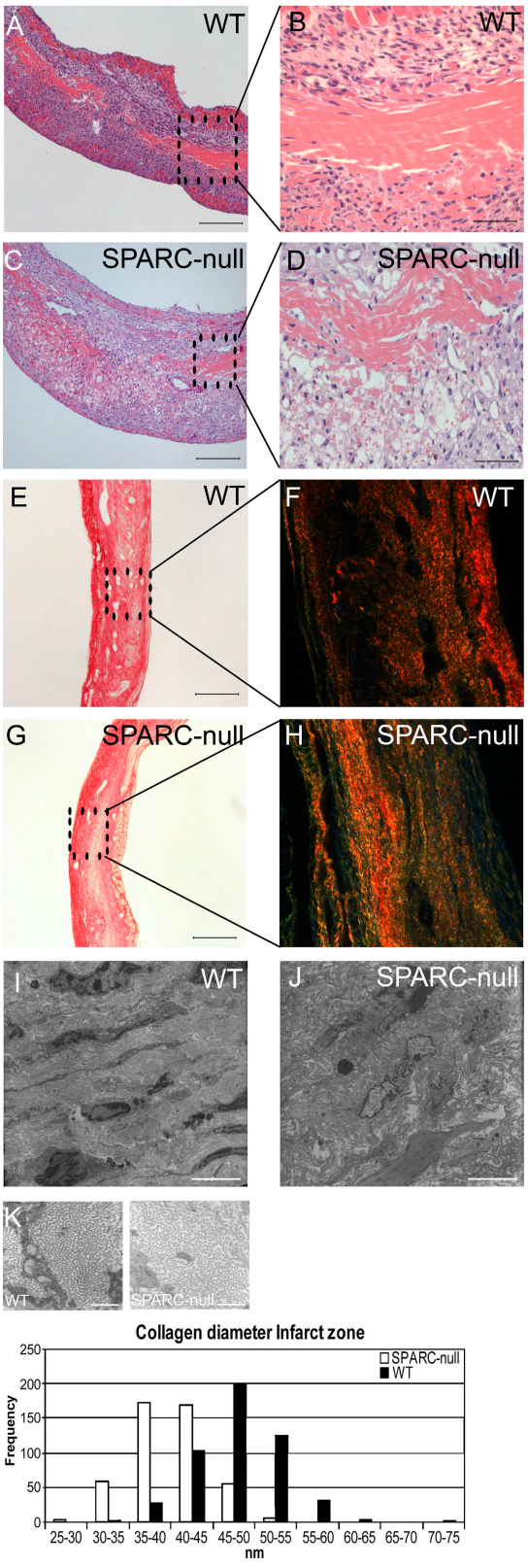

Figure 3. Adverse wound healing in *SPARC*-null mice. (A–D) Hematoxylin and eosin staining revealed a disorganized granulation tissue with increased RBC infiltration in male *SPARC*-null (C and D) versus WT (A and B) 7-d-old infarcts. (E–K) Abnormal collagen formation in *SPARC*-null infarcts. (E–H) Sirius red staining did not indicate substantial differences in the amount of collagen deposition between WT (E) and *SPARC*-null (G) infarcts at 14 d after MI. Sirius red polarization microscopy revealed well aligned and tightly packed (orange-red) collagen fibers in WT (F) but less mature fibers (yellow-green) in *SPARC*-null infarcts (H). (I–K) Ultrastructural analysis confirmed a disorganized matrix in *SPARC*-null (J) in comparison with WT (I) infarcts, which was associated with the deposition of smaller collagen fibrils in the infarct zone of *SPARC*-null mice (K; $n = 3$). Bars: (A, C, E, and G) 200 µm; (B and D) 50 µm; (I and J) 5 µm; (K) 500 nm.

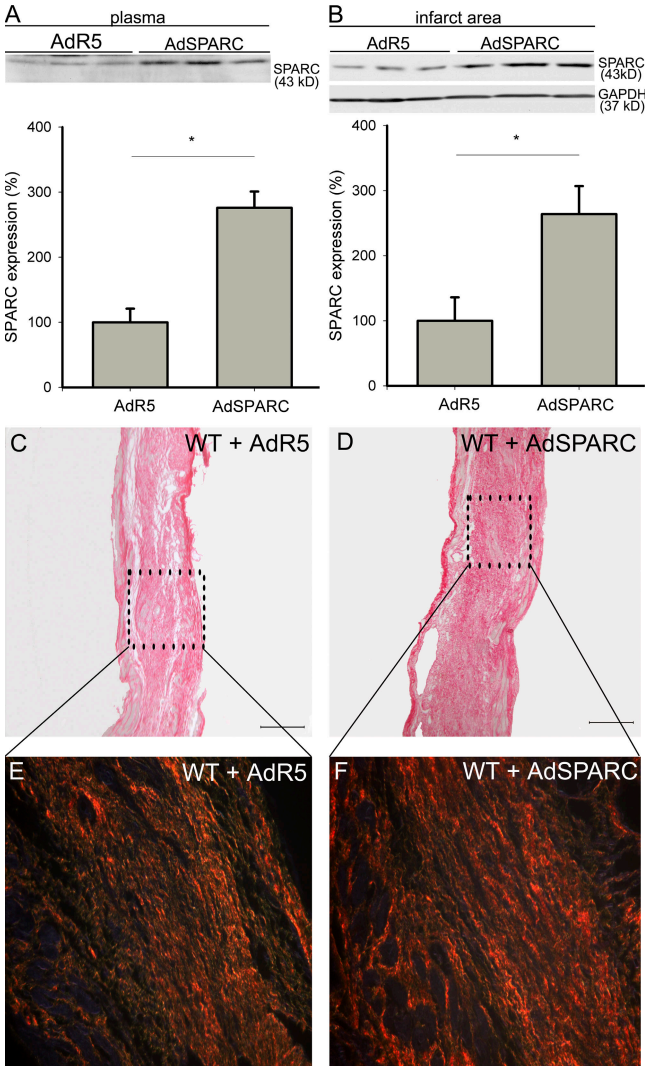

Figure 4. *SPARC* overexpression increases collagen deposition and quality after MI. (A and B) Representative Western blots showing a 2.8-fold increase of SPARC in plasma (A) and a 2.6-fold increase of SPARC in the infarct area (B) of AdSPARC-treated WT mice in comparison with AdR5-treated WT mice at 14 d after MI ($n = 4$; *, $P < 0.05$). (C–F) Sirius red staining and polarization microscopy revealed increased collagen deposition in AdSPARC-treated (D) in comparison with AdR5-treated WT infarcts (C) and more well aligned and tightly packed (orange-red) collagen fibers in AdSPARC-treated (F) in comparison with AdR5-treated WT infarcts (E). Error bars represent the mean ± SEM. Bars: (C and D) 2 mm; (E and F) 200 µm.

Table IV. Functional analysis of WT mice treated with AdR5 or AdSPARC virus

	Sham		MI, 14 d	
	AdR5, *n* = 4	AdSPARC, *n* = 4	AdR5, *n* = 9	AdSPARC, *n* = 9
FS (%)	22 ± 2.5	30 ± 2.0[a]	10 ± 1.7[a]	24 ± 3.4[b]
LVIDd (mm)	3.9 ± 0.1	4.1 ± 0.1	5.8 ± 0.2[a]	5.0 ± 0.2[ab]
LVIDs (mm)	3.0 ± 0.1	2.9 ± 0.1	5.2 ± 0.2[a]	3.8 ± 0.3[ab]
PWd (mm)	0.7 ± 0.1	0.7 ± 0.1	0.7 ± 0.1	0.8 ± 0.1[b]
IVSd (mm)	0.7 ± 0.1	0.7 ± 0.1	0.6 ± 0.1	0.7 ± 0.1[b]
HW/BW	3.9 ± 0.1	4.3 ± 0.2	5.1 ± 0.2[a]	4.8 ± 0.1[a]
LW/BW	5.7 ± 0.1	5.5 ± 0.1	7.0 ± 0.5[a]	5.3 ± 0.1[b]

FS, fractional shortening; LVIDd, left ventricular internal diameter diastole; LVIDs, left ventricular internal diameter systole; PWd, posterior wall diastole IVSd, intraventricular septum diastole; HW, heart weight; BW, body weight; and LW, lung weight.
[a]$P < 0.05$ in infarcted (MI) versus sham-operated mice or AdR5 versus AdSPARC sham-operated mice.
[b]$P < 0.05$ in AdvSPARC infarcts versus AdR5 infarcts.

analysis revealed increased deposition of collagen in TGF-β–treated compared with saline-treated *SPARC*-null hearts (Fig. 5, E–L; Table III), but no significant differences in inflammation or blood vessel formation were observed (Table III). Improved collagen maturation by infusion of TGF-β into *SPARC*-null infarcted mice was demonstrated by the significantly increased numbers of thick orange-red collagen fibers (ratio of orange-red/yellow-green birefringent collagen, 4.5 ± 1.2 in TGF-β–treated compared with 2.2 ± 0.4 in saline-treated *SPARC*-null infarcted mice; $n = 7$; $P < 0.05$; Fig. 5, E–L; Table III). Administration of TGF-β did not significantly affect wound healing or collagen formation in WT animals (Fig. 5, E–L; Table III).

DISCUSSION

This study indicates a crucial role for SPARC in infarct healing and collagen formation after MI. The absence of *SPARC* was associated with adverse healing and deficient maturation of collagen with increased cardiac rupture and dysfunction after MI. Importantly, adenoviral-mediated overexpression of *SPARC* (AdSPARC) in WT mice, resulting in increased plasma and cardiac levels of SPARC, improved collagen maturation and prevented cardiac dysfunction and dilatation after MI. Moreover, treatment with TGF-β prevented cardiac rupture in *SPARC*-null infarcted mice, a result which underscores our data in vitro and in vivo showing that exogenous SPARC regulates TGF-β signaling.

Expression of SPARC increases progressively after MI and is seen primarily in inflammatory cells and fibroblasts (1, 4), data which indicates a role for SPARC during healing of the infarct scar. The increased cardiac rupture and dysfunction that we observed appeared to coincide with the disorganized and fragmented granulation tissue as well as abnormal collagen maturation. Cardiac rupture mainly occurred in male mice. Hormonal status, higher blood pressure, and increased physical activity during the night may predispose to the increased cardiac rupture, dysfunction, and mortality in male compared with female mice after MI (13–16). To investigate whether differences in expression of SPARC or SPARC-related factors may influence the phenotype seen after MI, we determined transcript levels of *SPARC* and the SPARC-related factors *SMOC1*, *SMOC2*, and *Hevin* in males and females of both genotypes. Because these SPARC-related factors are expressed in the heart (9–11) and Hevin is involved in collagen assembly (17), these proteins may be implicated in infarct remodeling. Lack of *SPARC* did not result in compensatory changes of SPARC-related factors. However, sham WT and *SPARC*-null female mice displayed increased

Table V. Histological analysis of the infarcted area of AdR5- and AdSPARC-treated mice

	AdR5 MI, 14 d (*n* = 9)	AdSPARC MI, 14 d (*n* = 9)
Infarct size (%)	35 ± 3.9	38 ± 1.4
Residual necrotic area (%)	1.5 ± 2.3	2.1 ± 1.5
Infarct thickness (μm)	450 ± 16	520 ± 28
Leukocyte infiltration (cells/mm^2)	570 ± 91	560 ± 91
Coronary growth (vessels/mm^2)	32 ± 4	35 ± 3
Capillary growth (vessels/mm^2)	106 ± 11	113 ± 9
Myofibroblast (% area)	1.0 ± 0.2	1.6 ± 0.2
Collagen deposition (%)	28 ± 2.3	40 ± 2.5[a]
Ratio O-R thick/Y-G thin collagen fibers	18 ± 3.7	60 ± 11[a]

O-R, orange-red; Y-G, yellow-green.
[a]$P < 0.05$ in AdvSPARC infarcts versus AdR5 infarcts.

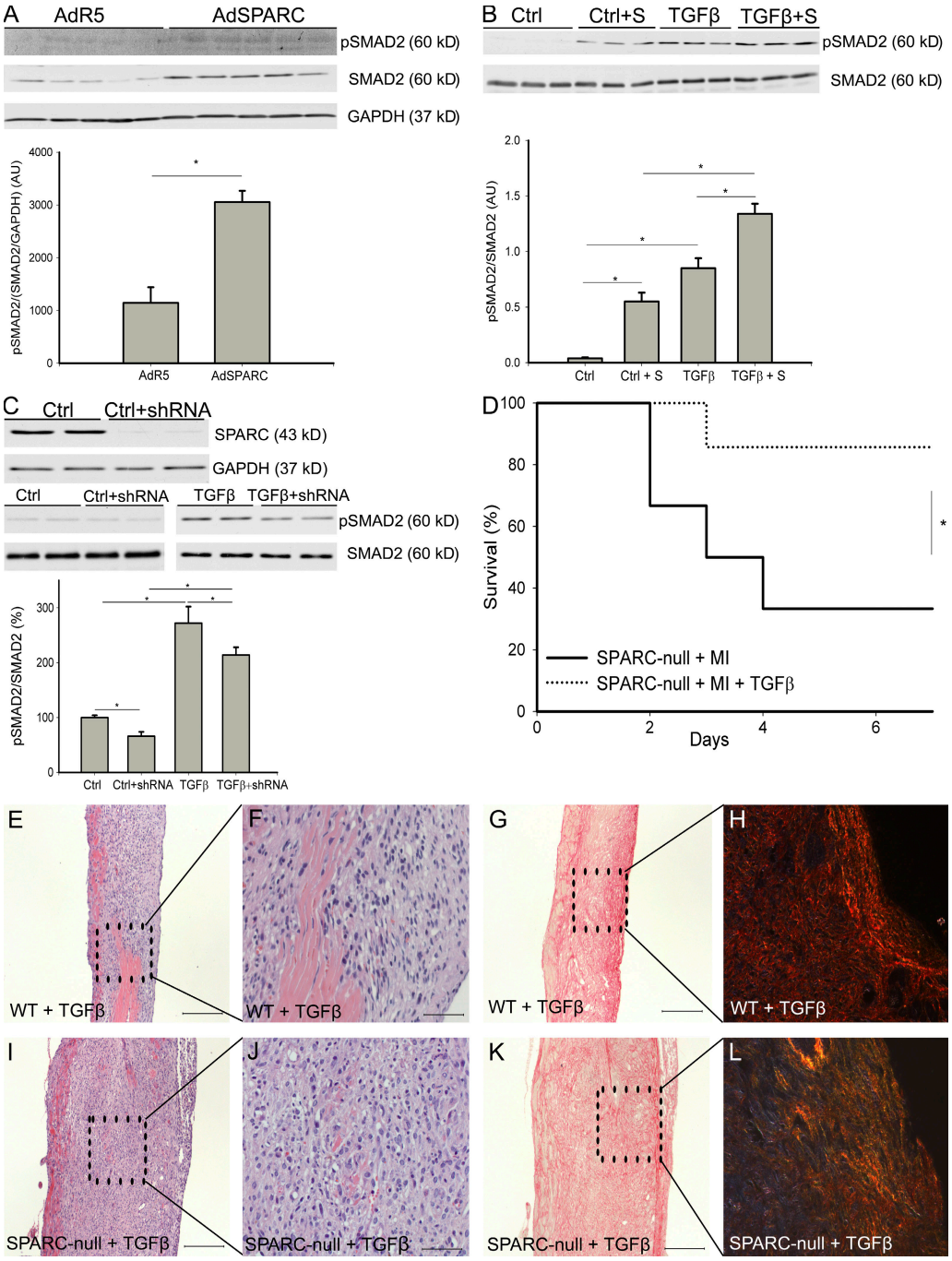

Figure 5. SPARC and TGF-β cooperate during infarct healing. (A) Representative Western blot showing increased phosphorylated and total Smad2 levels in the infarcts of AdSPARC-treated mice ($n = 9$; *, $P < 0.05$). (B) Representative Western blot showing that addition of recombinant mouse SPARC activated Smad2 signaling and augmented the Smad2-activating potential of TGF-β ($n = 6$; *, $P < 0.05$). (C) The top blot is a representative Western blot indicating that shRNA against SPARC resulted in an 80% decrease in levels of SPARC protein. The blots are representative Western blots showing that Smad2 phosphorylation in shRNA-treated cardiac fibroblasts was significantly decreased at baseline levels (left) and after 15 min of stimulation by 1 ng/ml TGF-β (right; $n = 5$ per group; *, $P < 0.05$). (D) Survival curve showing that infusion of TGF-β protected against cardiac rupture after MI in male *SPARC*-null mice (1 out of 7 mice) in comparison with saline-treated male *SPARC*-null mice (8 out of 12 mice; *, $P < 0.05$). (E, F, I, and J) Hematoxylin and eosin staining revealed striking differences between TGF-β–treated WT and *SPARC*-null mice 7 d after MI. In WT mice, infusion of TGF-β did not significantly affect wound healing, whereas in *SPARC*-null animals it stimulated ECM production in the infarct zone. (G, H, K, and L) Sirius Red staining and Sirius Red polarization microscopy revealed no apparent differences in collagen deposition between TGF-β1–treated *SPARC*-null and WT mice, whereas the difference in well aligned and tightly packed (orange-red) collagen fibers in WT infarcts (H), but less mature fibers (yellow-green) in *SPARC*-null infarcts (L), was preserved. Error bars represent the mean ± SEM. Bars: (E, G–I, K, and L) 200 µm; (F and J) 50 µm.

transcript levels of *SMOC2* in comparison with male sham mice. In contrast, *SMOC2* transcript levels did not differ significantly between the genders at 3 d after MI, indicating that SMOC2 may not protect female mice after MI. *SMOC1* transcript levels were strongly increased at 3 d after MI, suggesting that SMOC1 may be involved in regulation of the inflammatory response. Lack of clear differences in the expression pattern of *Hevin* at 3 d after MI precludes a significant role for this protein in cardiac rupture or early wound healing after MI. However, further investigation to delineate the specific roles of SPARC-related proteins in the pathogenesis of MI is mandatory.

We found that the total amount of collagen did not differ between *SPARC*-null and WT infarcts, but Sirius red polarization and electron microscopy revealed a disorganized and immature collagen matrix in the absence of SPARC. Importantly, infarcts from AdSPARC-treated WT mice displayed increased collagen deposition and improved maturation in comparison with infarcts of mice treated with control virus, data which clearly emphasizes the importance of SPARC for appropriate infarct healing.

SPARC likely regulates infarct healing and collagen maturation by several different mechanisms. First, SPARC directly interacts with collagen type I fibers (18, 19) and thereby affects their assembly. Variations in the structure of SPARC alter its affinity for collagen type I, and the absence of SPARC results in the formation of immature collagen fibers during wound healing in the skin (6) and in response to a foreign body (20). Moreover, *SPARC*-null fibroblasts lack the capacity to create a mature collagen matrix as a result of defects in procollagen processing (19). A second mechanism by which SPARC can regulate collagen matrix maturation is the capacity of SPARC to regulate fibronectin matrix assembly (21). In vitro, collagen fibril formation is dependent on the assembly of fibronectin into fibrils (22). Previous studies revealed that lack of *SPARC* results in impaired fibronectin unfolding, which is regulated via $\alpha_5\beta_1$ integrin and integrin-linked kinase, that could lead to the defective collagen maturation.

In this paper, we provide data that SPARC-mediated TGF-β1 signaling is important in regulating infarct healing in the heart. TGF-β1 is a cytokine involved in wound healing and collagen production, which produces multiple, and often opposing, cellular responses throughout the different phases of wound healing after MI (12). Two independent studies demonstrated that early inhibition of TGF-β signaling increased mortality and exacerbated LV dilatation and contractile dysfunction after MI, whereas blocking TGF-β signaling during a later phase prevented adverse LV remodeling (23, 24). We have now shown that SPARC regulates TGF-β signaling in cardiac fibroblasts and demonstrate that the increased TGF-β signaling in the infarct is beneficial for strengthening of the infarct scar. These findings are concordant with previous observations of SPARC-mediated TGF-β signaling in epithelial (25) and mesangial (8) cells. Our finding that treatment with TGF-β prevented infarct rupture and rescued collagen maturation in *SPARC*-null mice, but did not significantly affect infarct healing in WT animals, provides strong evidence in vivo for an important role for SPARC-mediated TGF-β signaling in infarct healing and collagen maturation after MI.

The importance of matricellular proteins and proteoglycans in cardiac wound healing and remodeling has previously been noted (26). These macromolecules, which are minimally expressed in the normal uninjured heart, are highly up-regulated in the injured heart. Recent publications have described roles for thrombospondin-1 (27), osteopontin (28), tenascin-C (29), and syndecan-1 (30) in wound healing of the infarcted heart. Thrombospondin-1 and syndecan-1, which are expressed early after MI, serve as a "barrier" limiting the influx of inflammatory cells and thereby regulate proper infarct healing and prevent infarct expansion and cardiac dilatation. In contrast, osteopontin (3, 28), tenascin-C (29), and SPARC (3, 4) are expressed principally during the formation of granulation tissue and fibrous scar and are implicated in the assembly and maturation of collagen fibers.

In conclusion, this is the first study to reveal that expression of SPARC after MI is essential for proper infarct healing and function after MI. SPARC should be considered as a novel therapeutic agent to improve cardiac remodeling and function after MI.

MATERIALS AND METHODS

Mouse model of MI. All described study protocols were approved by the Animal Care and Use Committee of the University of Maastricht and Leuven. Experiments were performed according to the official rules formulated in the Dutch and Belgian law on care and use of experimental animals. 130 10–18-wk-old male and female *SPARC*-null mice (backcrossed 10 times) and WT animals on a C57Bl6/J background were used in this study, and all experiments were performed using age-matched mice. Experimental MI and sham operation were performed as previously described (16). Hearts were perfused with PBS, removed, and prepared for molecular, histological, and ultrastructural analysis.

Histology and electron microscopy. Cardiac tissue was processed and histochemical and immunohistochemical analyses were performed as previously described (16, 30). Percentage of infarct size was expressed as the fractional circumference of the infarcted versus infarcted plus noninfarcted left ventricular wall and septum, which was assessed by measuring the midline circumference of three sections of the LV on hemalum eosin–stained sections. Infarct thickness (in micrometers) was measured as the mean of 20 measurements across the infarcted LV wall. Residual necrotic area was determined as the percentage of the total infarcted area. Myofibroblast infiltration was studied as the fractional areas of the infarct stained for α-SMC actin (DAKO), excluding coronary vessels. The number of CD-45–staining cells (BD), CD-31–staining capillaries (BD), and α-SMC actin–positive coronary vessels (Sigma-Aldrich) in the infarct zone was measured per mm^2. For colocalization studies, sections were subsequently incubated with Biotin-labeled secondary antibodies followed by amplification with the signal amplification system (streptavidin-HRP-C-fluorescein/Cy3; PerkinElmer) for SPARC (R&D Systems), CD45, and α-SMC. Nuclei were stained with DAPI (Invitrogen).

To assess the quality of the newly formed collagen matrix, Sirius Red staining was performed as previously described (30, 31). The quality of the newly deposited collagen matrix was studied with Sirius Red polarization microscopy, quantifying the ratio of the thick closely packed mature collagen fibers as orange-red birefringent to the loosely packed less cross-linked and immature collagen fibers as yellow-green birefringent (orange-red/yellow-green ratio).

All morphometric analyses were done in a standard way on two midsagittal sections of each heart. Morphometric analyses were performed using a microscope (Leitz DMRXE; Leica), and QWin morphometry software (Leica). Ultrastructural analysis was performed as previously described (20). All analyses were performed according to standard operating procedures and confirmed by independent observers blinded to genotype or treatment group.

Cardiac fibroblast culture and lentiviral constructs. Cardiac fibroblasts were isolated from 2-d-old neonatal Lewis rats. All the experiments were performed on second-passage cells. Cells were maintained in DME supplemented with 10% FBS and 0.1% gentamycin and were incubated at 37°C in a humidified chamber. shRNA against *SPARC* was produced from small interfering RNA (Eurogentec; Table S3, available at http://www.jem.org/cgi/content/full/jem.20081244/DC1) and cloned into the XhoI and HpaI sites of pLenti Lox 3.7 (32), and constructs were verified by sequencing. This vector was modified from the pLenti Lox 3.7 vector by replacement of the enhanced GFP gene by puromycin. Lentiviral production was performed by cotransfection of shSPARC/pLL3.7 or empty pLL3.7 puro with packaging vectors into 293FT cells by the use of Lipofectamine 2000 (Invitrogen). Virus-containing supernates were collected after 48 h. Reduction of *SPARC* mRNA in cardiac fibroblasts was achieved by treatment of rat fibroblasts with lentivirus containing shRNA against *SPARC* for 48 h. After selection in puromycin, cells were placed in medium containing 0.4% FBS for 24 h. Thereafter, fibroblasts were treated with 1 ng/ml TGF-β for 15 min.

Recombinant SPARC protein was produced by infection of CHO cells with adenovirus containing mouse *SPARC*. Serum-free media of these cells were collected, purified, and concentrated as described previously (33). Cardiac fibroblasts were placed in medium containing 0.4% FBS for 24 h, after which time 30 μg/ml of recombinant SPARC was added for 1 h. Hereafter, the cells were incubated with 1 ng/ml TGF-β for 15 min.

Western blotting. Infarcted tissue or cell lysates were resolved by SDS-PAGE and were subsequently immunoblotted for the detection of phosphorylated and total Smad2 (Cell Signaling Technology), SPARC (R&D systems), and GAPDH (Research Diagnostics, Inc.) as previously described (34). GAPDH was used as a loading control.

RNA isolation and expression. RNA was isolated from infarcted and sham tissue with the RNeasy Mini kit (QIAGEN) and was stored at −80°C. RNA was reverse transcribed into complementary DNA with the iScript cDNA synthesis kit (Bio-Rad Laboratories). Real-time quantitative PCR was performed with iQ SYBR green supermix (Bio-Rad Laboratories). Primers were designed with Primer Express software (Applied Biosystems). *Cyclophilin* or *acidic ribosomal phosphoprotein* was used as a housekeeping gene. The primers used are shown in Table S4 (available at http://www.jem.org/cgi/content/full/jem.20081244/DC1).

Echocardiography and functional assessments. After sedation of mice with 2% isoflurane, standard views were obtained in two-dimensional and M mode by transthoracic echocardiography with a 13-MHz transducer (i13L; GE Healthcare) on a GE Vivid7 (GE Healthcare) echocardiograph. Cardiac function was assessed with increasing dosages of dobutamine in intact female SPARC-null and WT mice 14 d after surgery under 2.5 g/kg urethane i.p. anesthesia as previously described (34).

Adenoviral overexpression of *SPARC*. *SPARC* overexpression was achieved by adenoviral infection of WT mice. The design of the adenoviral vector is described by Barker et al. (21). Adenovirus was produced by 293 cells that were collected and purified as previously described (35). 10^9 adenoviral PFU was injected into the tail vein 2 d before the onset of acute MI to achieve high levels of SPARC at the onset of MI. 1 d before MI, baseline echocardiography was performed. 2 wk after MI, echocardiography was performed and the mice were killed, after which histological and molecular analysis of infarcted hearts was performed. Overexpression of SPARC was shown by immunoblotting of the plasma of mice that had been treated with SPARC adenovirus.

TGF-β infusion in SPARC-null and WT mice. To investigate whether exogenous administration of TGF-β rescued increased cardiac rupture after MI, we treated SPARC-null and WT mice with 250 ng/d TGF-β versus saline for 7 d using osmotic minipumps.

Statistical analysis. Data were expressed as the mean ± SEM. No repeated measures were performed. Echocardiographic measurements and histological and molecular analysis in sham-operated and infarcted groups at 3, 7, and 14 d were performed in independent groups. Normal distribution of all continuous variables was tested according to the method of Kolmogorov and Smirnov. An unpaired Student's *t* test was used in most of the comparisons when groups passed the normality test.

A Mann-Whitney test was used when the SD of two groups significantly differed. A two-way ANOVA was used for comparison of the dobutamine curves. Survival curves after MI were obtained by the Kaplan-Meier method and compared by the log-rank test. A two-sided p-value of <0.05 was considered statistically significant.

Online supplemental material. Table S1 shows the transcript levels of ECM mRNAs in sham and infarcted WT and *SPARC*-null mice. Table S2 shows the transcript levels of ECM mRNAs in sham and infarcted AdR5- and AdSPARC-treated WT mice, confirming increased ECM deposition in AdSPARC-treated infarcts. Table S3 shows the sequences used for the creation of shRNA against SPARC. Table S4 shows the primers used with real-time PCR. Online supplemental material is available at http://www.jem.org/cgi/content/full/jem.20081244/DC1.

This study was supported by a research grant of the Netherlands Heart Foundation (NHS; 2005B082, 2007B036, and 2008B011) to S. Heymans, an Ingenious Hypercare NoE EU grant to S. Heymans, a Research grant of the Research fund K.U. Leuven (PDMK/08/175) to D. Vanhoutte, and National Institutes of Health grant GM-40711 to E.H. Sage. Y.M. Pinto is an established investigator of the Netherlands Heart Foundation.

The authors have no conflicting financial interests.

Submitted: 6 June 2008
Accepted: 21 November 2008

REFERENCES

1. Framson, P.E., and E.H. Sage. 2004. SPARC and tumor growth: where the seed meets the soil? *J. Cell. Biochem.* 92:679–690.
2. Bradshaw, A.D., and E.H. Sage. 2001. SPARC, a matricellular protein that functions in cellular differentiation and tissue response to injury. *J. Clin. Invest.* 107:1049–1054.
3. Dobaczewski, M., M. Bujak, P. Zymek, G. Ren, M.L. Entman, and N.G. Frangogiannis. 2006. Extracellular matrix remodeling in canine and mouse myocardial infarcts. *Cell Tissue Res.* 324:475–488.
4. Komatsubara, I., T. Murakami, S. Kusachi, K. Nakamura, S. Hirohata, J. Hayashi, S. Takemoto, C. Suezawa, Y. Ninomiya, and Y. Shiratori. 2003. Spatially and temporally different expression of osteonectin and osteopontin in the infarct zone of experimentally induced myocardial infarction in rats. *Cardiovasc. Pathol.* 12:186–194.
5. Basu, A., L.H. Kligman, S.J. Samulewicz, and C.C. Howe. 2001. Impaired wound healing in mice deficient in a matricellular protein SPARC (osteonectin, BM-40). *BMC Cell Biol.* 2:15.
6. Bradshaw, A.D., M.J. Reed, and E.H. Sage. 2002. SPARC-null mice exhibit accelerated cutaneous wound closure. *J. Histochem. Cytochem.* 50:1–10.
7. Lindsey, M.L., D.L. Mann, M.L. Entman, and F.G. Spinale. 2003. Extracellular matrix remodeling following myocardial injury. *Ann. Med.* 35:316–326.
8. Francki, A., T.D. McClure, R.A. Brekken, K. Motamed, C. Murri, T. Wang, and E.H. Sage. 2004. SPARC regulates TGF-beta1-dependent signaling in primary glomerular mesangial cells. *J. Cell. Biochem.* 91:915–925.
9. Soderling, J.A., M.J. Reed, A. Corsa, and E.H. Sage. 1997. Cloning and expression of murine SC1, a gene product homologous to SPARC. *J. Histochem. Cytochem.* 45:823–835.

10. Vannahme, C., S. Gosling, M. Paulsson, P. Maurer, and U. Hartmann. 2003. Characterization of SMOC-2, a modular extracellular calcium-binding protein. *Biochem. J.* 373:805–814.
11. Vannahme, C., N. Smyth, N. Miosge, S. Gosling, C. Frie, M. Paulsson, P. Maurer, and U. Hartmann. 2002. Characterization of SMOC-1, a novel modular calcium-binding protein in basement membranes. *J. Biol. Chem.* 277:37977–37986.
12. Bujak, M., and N.G. Frangogiannis. 2006. The role of TGF-beta signaling in myocardial infarction and cardiac remodeling. *Cardiovasc. Res.* 74:184–195.
13. Cavasin, M.A., S.S. Sankey, A.L. Yu, S. Menon, and X.P. Yang. 2003. Estrogen and testosterone have opposing effects on chronic cardiac remodeling and function in mice with myocardial infarction. *Am. J. Physiol. Heart Circ. Physiol.* 284:H1560–H1569.
14. Cavasin, M.A., Z.Y. Tao, A.L. Yu, and X.P. Yang. 2006. Testosterone enhances early cardiac remodeling after myocardial infarction, causing rupture and degrading cardiac function. *Am. J. Physiol. Heart Circ. Physiol.* 290:H2043–H2050.
15. Gao, X.M., Q. Xu, H. Kiriazis, A.M. Dart, and X.J. Du. 2005. Mouse model of post-infarct ventricular rupture: time course, strain- and gender-dependency, tensile strength, and histopathology. *Cardiovasc. Res.* 65:469–477.
16. Heymans, S., A. Luttun, D. Nuyens, G. Theilmeier, E. Creemers, L. Moons, G.D. Dyspersin, J.P. Cleutjens, M. Shipley, A. Angellilo, et al. 1999. Inhibition of plasminogen activators or matrix metalloproteinases prevents cardiac rupture but impairs therapeutic angiogenesis and causes cardiac failure. *Nat. Med.* 5:1135–1142.
17. Sullivan, M.M., T.H. Barker, S.E. Funk, A. Karchin, N.S. Seo, M. Hook, J. Sanders, B. Starcher, T.N. Wight, P. Puolakkainen, and E.H. Sage. 2006. Matricellular hevin regulates decorin production and collagen assembly. *J. Biol. Chem.* 281:27621–27632.
18. Kaufmann, B., S. Muller, F.G. Hanisch, U. Hartmann, M. Paulsson, P. Maurer, and F. Zaucke. 2004. Structural variability of BM-40/SPARC/osteonectin glycosylation: implications for collagen affinity. *Glycobiology.* 14:609–619.
19. Rentz, T.J., F. Poobalarahi, P. Bornstein, E.H. Sage, and A.D. Bradshaw. 2007. SPARC regulates processing of procollagen I and collagen fibrillogenesis in dermal fibroblasts. *J. Biol. Chem.* 282:22062–22071.
20. Puolakkainen, P., A.D. Bradshaw, T.R. Kyriakides, M. Reed, R. Brekken, T. Wight, P. Bornstein, B. Ratner, and E.H. Sage. 2003. Compromised production of extracellular matrix in mice lacking secreted protein, acidic and rich in cysteine (SPARC) leads to a reduced foreign body reaction to implanted biomaterials. *Am. J. Pathol.* 162:627–635.
21. Barker, T.H., G. Baneyx, M. Cardo-Vila, G.A. Workman, M. Weaver, P.M. Menon, S. Dedhar, S.A. Rempel, W. Arap, R. Pasqualini, et al. 2005. SPARC regulates extracellular matrix organization through its modulation of integrin-linked kinase activity. *J. Biol. Chem.* 280:36483–36493.
22. Velling, T., J. Risteli, K. Wennerberg, D.F. Mosher, and S. Johansson. 2002. Polymerization of type I and III collagens is dependent on fibronectin and enhanced by integrins alpha 11beta 1 and alpha 2beta 1. *J. Biol. Chem.* 277:37377–37381.
23. Ikeuchi, M., H. Tsutsui, T. Shiomi, H. Matsusaka, S. Matsushima, J. Wen, T. Kubota, and A. Takeshita. 2004. Inhibition of TGF-beta signaling exacerbates early cardiac dysfunction but prevents late remodeling after infarction. *Cardiovasc. Res.* 64:526–535.
24. Okada, H., G. Takemura, K. Kosai, Y. Li, T. Takahashi, M. Esaki, K. Yuge, S. Miyata, R. Maruyama, A. Mikami, et al. 2005. Postinfarction gene therapy against transforming growth factor-beta signal modulates infarct tissue dynamics and attenuates left ventricular remodeling and heart failure. *Circulation.* 111:2430–2437.
25. Schiemann, B.J., J.R. Neil, and W.P. Schiemann. 2003. SPARC inhibits epithelial cell proliferation in part through stimulation of the transforming growth factor-beta-signaling system. *Mol. Biol. Cell.* 14:3977–3988.
26. Schellings, M.W., Y.M. Pinto, and S. Heymans. 2004. Matricellular proteins in the heart: possible role during stress and remodeling. *Cardiovasc. Res.* 64:24–31.
27. Frangogiannis, N.G., G. Ren, O. Dewald, P. Zymek, S. Haudek, A. Koerting, K. Winkelmann, L.H. Michael, J. Lawler, and M.L. Entman. 2005. Critical role of endogenous thrombospondin-1 in preventing expansion of healing myocardial infarcts. *Circulation.* 111:2935–2942.
28. Trueblood, N.A., Z. Xie, C. Communal, F. Sam, S. Ngoy, L. Liaw, A.W. Jenkins, J. Wang, D.B. Sawyer, O.H. Bing, et al. 2001. Exaggerated left ventricular dilation and reduced collagen deposition after myocardial infarction in mice lacking osteopontin. *Circ. Res.* 88:1080–1087.
29. Tamaoki, M., K. Imanaka-Yoshida, K. Yokoyama, T. Nishioka, H. Inada, M. Hiroe, T. Sakakura, and T. Yoshida. 2005. Tenascin-C regulates recruitment of myofibroblasts during tissue repair after myocardial injury. *Am. J. Pathol.* 167:71–80.
30. Vanhoutte, D., M.W. Schellings, M. Gotte, M. Swinnen, V. Herias, M.K. Wild, D. Vestweber, E. Chorianopoulos, V. Cortes, A. Rigotti, et al. 2007. Increased expression of syndecan-1 protects against cardiac dilatation and dysfunction after myocardial infarction. *Circulation.* 115:475–482.
31. Junqueira, L.C., G. Bignolas, and R.R. Brentani. 1979. Picrosirius staining plus polarization microscopy, a specific method for collagen detection in tissue sections. *Histochem. J.* 11:447–455.
32. Rubinson, D.A., C.P. Dillon, A.V. Kwiatkowski, C. Sievers, L. Yang, J. Kopinja, D.L. Rooney, M.M. Ihrig, M.T. McManus, F.B. Gertler, et al. 2003. A lentivirus-based system to functionally silence genes in primary mammalian cells, stem cells and transgenic mice by RNA interference. *Nat. Genet.* 33:401–406.
33. Sage, E.H. 2003. Purification of SPARC/osteonectin. *Curr. Protoc. Cell Biol.* DOI:10.1002/0471143030.cb1011s17.
34. Schellings, M.W., M. Baumann, R.E. van Leeuwen, R.F. Duisters, S.H. Janssen, B. Schroen, C.J. Peutz-Kootstra, S. Heymans, and Y.M. Pinto. 2006. Imatinib attenuates end-organ damage in hypertensive homozygous TGR(mRen2)27 rats. *Hypertension.* 47:467–474.
35. He, T.C., S. Zhou, L.T. da Costa, J. Yu, K.W. Kinzler, and B. Vogelstein. 1998. A simplified system for generating recombinant adenoviruses. *Proc. Natl. Acad. Sci. USA.* 95:2509–2514.